Bioorg. Med. Chem. 56 (2022) 116588

Contents lists available at ScienceDirect

Bioorganic & Medicinal Chemistry

journal homepage: www.elsevier.com/locate/bmc

Using *in vitro* ADME data for lead compound selection: An emphasis on PAMPA pH 5 permeability and oral bioavailability

Jordan Williams, Vishal Siramshetty, Đắc-Trung Nguyễn [1], Elias Carvalho Padilha, Md. Kabir [2], Kyeong-Ri Yu [3], Amy Q. Wang, Tongan Zhao, Misha Itkin, Paul Shinn, Ewy A. Mathé, Xin Xu, Pranav Shah [*]

National Center for Advancing Translational Sciences (NCATS), 9800 Medical Center Drive, Rockville, MD 20850, United States

ARTICLE INFO

Keywords:
Quantitative structure activity relationship
PAMPA
ADME
Oral bioavailability
Machine learning
In silico models

ABSTRACT

Membrane permeability plays an important role in oral drug absorption. Caco-2 and Madin-Darby Canine Kidney (MDCK) cell culture systems have been widely used for assessing intestinal permeability. Since most drugs are absorbed passively, Parallel Artificial Membrane Permeability Assay (PAMPA) has gained popularity as a low-cost and high-throughput method in early drug discovery when compared to high-cost, labor intensive cell-based assays. At the National Center for Advancing Translational Sciences (NCATS), PAMPA pH 5 is employed as one of the Tier I absorption, distribution, metabolism, and elimination (ADME) assays. In this study, we have developed a quantitative structure activity relationship (QSAR) model using our ~6500 compound PAMPA pH 5 permeability dataset. Along with ensemble decision tree-based methods such as Random Forest and eXtreme Gradient Boosting, we employed deep neural network and a graph convolutional neural network to model PAMPA pH 5 permeability. The classification models trained on a balanced training set provided accuracies ranging from 71% to 78% on the external set. Of the four classifiers, the graph convolutional neural network that directly operates on molecular graphs offered the best classification performance. Additionally, an ~85% correlation was obtained between PAMPA pH 5 permeability and *in vivo* oral bioavailability in mice and rats. These results suggest that data from this assay (experimental or predicted) can be used to rank-order compounds for preclinical *in vivo* testing with a high degree of confidence, reducing cost and attrition as well as accelerating the drug discovery process. Additionally, experimental data for 486 compounds (PubChem AID: 1645871) and the best models have been made publicly available (https://opendata.ncats.nih.gov/adme/).

1. Introduction

Absorption is a critical property for orally administered drugs, as the drug must pass through the intestinal epithelium before reaching systemic circulation. Absorption is not only dependent upon the characteristics of the gastrointestinal (GI) tract, but also on physicochemical properties of the drug.[1–3] Several studies have shown that absorption of drugs is regional[4,5] and pH gradient in the intestinal tract (from acidic, i.

Abbreviations: 5-CV, 5-fold cross validation; ACN, Acetonitrile; ADME, Absorption, Distribution, Metabolism, Excretion; AI, Artificial Intelligence; ANN, Artificial Neural Network; AUC, Area Under the Curve; BACC, Balanced Accuracy; DMSO, Dimethyl sulfoxide; DNN, Deep Neural Network; GBM, Generalized Boosted Models; GCNN, Graph Convolutional Neural Network; GI, Gastrointestinal; IV, Intravenous; MDCK, Madin-Darby Canine Kidney cells; ML, Machine Learning; MSR, Minimum Significant Ratio; MW, Molecular Weight; NCATS, National Center for Advancing Translational Sciences; PAMPA, Parallel Artificial Membrane Permeability Assay; PEOE, Partial Equalization of Orbital Electronegativities; PK, Pharmacokinetic; PLS, Partial Least Squares; PO, Per Os (orally administered); QSAR, Quantitative Structure Activity Relationship; RF, Random Forest; ROC, Receiver Operating Characteristic; S.D., Standard Deviation; TPSA, Total Polar Surface Area; UPLC/MS, Ultra-high Performance Liquid Chromatography Mass Spectrometry; UV, Ultraviolet; XGBoost, eXtreme Gradient Boosting.

* Corresponding author.
E-mail address: pranav.shah@nih.gov (P. Shah).
[1] Present address: Worldwide Research, Development and Medical, Pfizer Inc., USA.
[2] Present address: The Graduate School of Biomedical Sciences, Icahn School of Medicine at Mount Sinai, 1 Gustave L. Levy Place, New York, NY 10029, United States.
[3] Present address: Department of Surgery, Virginia Commonwealth University Health Systems, 1200 E Broad St, Richmond, VA 23298, United States.

https://doi.org/10.1016/j.bmc.2021.116588
Received 7 October 2021; Received in revised form 13 December 2021; Accepted 19 December 2021
Available online 5 January 2022

e., pH 2–3 to basic i.e., pH 8–9) has been attributed as a major influencing factor.[6,7] For example, most intestinal absorption occurs in the small intestine (the duodenum, jejunum, and ileum specifically) where pH ranges from 4-7.[8] This phenomenon is explained by the pH-partition hypothesis which states that only uncharged compounds can permeate through the lipophilic membrane.[9] This suggests that permeability of a compound would vary across different segments of the GI tract depending on pH and permeability of a compound would be greatest at the pH where it is least charged.

Two of the most popular cellular *in vitro* membrane permeability methods used in drug discovery include Caco-2 and Madin-Darby Canine Kidney (MDCK) monolayer assays. Caco-2 is a human epithelial colon adenocarcinoma cell line which presents both enterocytic and colonocytic[10] characteristics. Additionally, data generated in these cells exhibit good correlation with *in vivo* bioavailability[11] and permeability like that of the human jejunum.[12] MDCK cells, isolated from canine distal renal tissue, came in later as a faster and more cost-effective alternative to Caco-2 cells.[13] While these cell lines model active and passive transport, their use is often limited due to high costs, long membrane growth cycles (21-day and 5-day culture time for Caco-2 and MDCK cells respectively), lab-to-lab and batch-to-batch variation.[14–16] In addition to cell-based assays, Parallel Artificial Membrane Permeability Assay (PAMPA) is also popular as a cost-effective, non-cell-based screening tool.[17–19] One of the major disadvantages of PAMPA (i.e., its inability to model active transport[20,18]) is offset by the fact that more than 90% of drugs are absorbed via passive diffusion.[21,2,22,17,20] PAMPA permeability at both pH 7.4 and pH 5.5 correlates well with Caco-2 permeability in small data sets.[23] The adaptability of PAMPA to high-throughput in combination with its flexibility with experimental conditions (different lipid compositions/range of pH conditions) makes PAMPA an excellent screening method in early drug discovery. This technique has been extensively used in several published drug discovery projects with a great deal of success.[24–30] While it is extremely important to study the pH-permeability relationship especially for ionizable compounds, there is a dearth of PAMPA data in literature especially at non-neutral pH.[18–19,22–23] At the National Center for Advancing Translational Sciences (NCATS), compounds are routinely screened for permeability using a high-throughput, double-sink PAMPA assay at pH 5. On examining the correlation between PAMPA pH 5 permeability and preclinical oral bioavailability using in-house pharmacokinetic (PK) datasets, a correlation of ~85% was determined, further underlining the importance of this assay as a screening tool in drug discovery.

The current cost of bringing a new drug from drug discovery through to the market stands at $2.6 billion USD.[31] This cost has risen steadily throughout the last few decades, making it critical to find alternatives to reduce costs in the drug discovery process. Quantitative structure activity relationships (QSAR) using machine learning approaches, a branch of artificial intelligence (AI), has been shown to improve the decision-making process across various steps in drug discovery, including its use in predicting PAMPA permeability. While a few PAMPA QSAR models do exist, they are primarily based on small datasets and in most cases neither the data nor the models are made publicly available.[1,2,32,33,19] In this study, we present an *in silico* model for predicting drug permeability at pH 5 based on experimental PAMPA data collected at NCATS, a complement to our previously published PAMPA pH 7.4 model.[18] The PAMPA pH 5 model features a dataset of ~6500 compounds, representing a variety of small molecule drug discovery projects and chemotypes. We employed both classical and advanced machine learning techniques to develop the prediction models. The best model with both training and validation accuracies over 75% was made available on the publicly accessible NCATS ADME portal (https://opendata.ncats.nih.gov/adme/), which can be useful in rank-ordering virtual compounds for their potential behavior in a PAMPA pH 5 assay and identifying compounds with poor permeability profiles.

2. Materials & methods

2.1. Materials and instrumentation

2.1.1. Materials

Dimethyl sulfoxide (DMSO, ultra-high performance liquid chromatography mass spectrometry (UPLC/MS) grade), ammonium acetate, sodium hydroxide, ranitidine, dexamethasone, verapamil, and albendazole were purchased from Sigma-Aldrich (St. Louis, MO). Acetonitrile (ACN, UPLC/MS grade) was purchased from Fisher Scientific (Hampton, NH). GIT-0 lipid (Catalog #110669), acceptor sink buffer (pH 7.4, Catalog #110139), PRISMA HT buffer (Catalog #110151), 96-well stirwell sandwich plates with stirrers (Catalog #120551-SUPP), and high sensitivity ultraviolet (UV) plates (Catalog #110286) were purchased from Pion Inc. (Billerica, MA).

2.1.2. Instrumentation

Experiments were performed using a Freedom Evo 200 automated platform with a 96-channel (MCA96) head and 8-channel liquid handling (LiHa) system with EVOware software (version 2.3) (Tecan Inc., Männedorf, Switzerland). The system also includes a Gutbox (Pion Inc.) and a Nano Quant Infinite 200 Pro UV plate reader (Tecan Inc.). 200 μL pipette tips (MCA96: Catalog #14–223-552, Fisher Scientific, Hampton, NH; LiHa: Catalog #110126, Pion Inc., Billerica, MA) were used in the experiments.

2.2. PAMPA permeability pH 5 method

The stirring double-sink PAMPA method (patented by Pion Inc.) was employed to determine the permeability of compounds in a high-throughput format.[17] The GIT-0 lipid (proprietary Pion Inc. lipid, optimized to predict GI tract passive permeability) was immobilized on the 0.45 μm PVDF matrix of a 96-well "acceptor" filter plate placed atop a 96-well "donor" plate. pH 5 buffer (PRISMA HT buffer; made by diluting 50 mL of the buffer to 2000 mL with water and adjusting pH as needed), was used in the donor wells and pH 7.4 buffer (acceptor sink buffer) was used in the acceptor wells. The test articles (in duplicates), stocked in 10 mM DMSO solutions, were diluted to 0.05 mM in aqueous buffer (PRISMA HT pH 5), and the concentration of DMSO was $< 0.5\%$ in the final solution. During the 30-minute incubation at room temperature, test samples in the donor compartment were stirred using Gutbox technology (Pion Inc.) to reduce the aqueous boundary layer. The test article concentrations in the donor and acceptor compartments were then measured using a UV plate reader (Nano Quant, Infinite 200 PRO, Tecan Inc., Männedorf, Switzerland). Calculations were performed using Pion Inc. software and effective permeability (P_{eff}) was expressed in units of 10^{-6} cm/s. If the permeability could not be determined via UV, the samples were plated for analysis via UPLC/MS by plating 8 μL of the incubation solutions in 192 μL of ACN/Internal Standard (albendazole) solution in a 96-well plate (350 μL, Waters, Milford, MA). A previously published ultra-high performance liquid chromatography mass spectrometry method, with minor modifications, was used to analyze the samples.[34] PAMPA pH 7.4 assays were performed as previously published.[18]

2.3. Compound data sets

A total of 6500 measurements were available in the PAMPA pH 5 assay. These compounds were synthesized at NCATS and they represent a variety of small molecule drug discovery projects and chemotypes. Compounds were categorized with the following cutoffs: low permeability: $<10 \times 10^{-6}$ cm/s and moderate/high permeability: $>10 \times 10^{-6}$ cm/s. For the model, compound structures were standardized following best practices recommended in the literature.[35] LyChI hash identifiers (https://github.com/ncats/lychi) were generated for all standardized structures to group them into unique compounds. For compounds with

multiple measurements, the values were averaged if all values fell within the same category and compounds with conflicting experimental results were omitted. Finally, the processed data set comprised a total of 5227 unique compounds. The data set was randomly divided into a training set (80%; 4181 compounds labelled as Training set I) used to build the models and an external set (20%; 1046 compounds) used to validate the models. 486 out of 5277 compounds were identified as open access compounds and PAMPA pH 5 data for these compounds have been deposited on PubChem (AID: 1645871) as part of this study. The remaining 4741 compounds were identified as part of on-going projects at NCATS and data for these compounds will be released at some point in the future.

Due to imbalance in the distribution of training set compounds between the two classes (low permeability and moderate/high permeability), we decided to generate a balanced training set using the diversity under-sampling method.[36] Retaining all minority class (i.e., low permeability) compounds, a structurally diverse set of majority class compounds that is double the size of the minority class was obtained using RDKit Diversity Picker node in KNIME. Using this technique, a total of 1698 compounds were used as a balanced dataset (not to be confused with a perfectly balanced dataset; labelled as Training set II) to generate the same set of models. The same external set was employed for validating these models to mimic the imbalanced nature of the data in a realistic setting. An overview of the training and external data sets is provided in Table 1.

2.4. Molecular descriptors

We used molecular descriptors available from the RDKit toolkit (https://www.rdkit.org/; version 2020.03.1) as one of the input features. Each compound in the data set is represented by a total of 119 RDKit descriptors. In addition, molecular fingerprints (bit vector representations of molecules) that encode substructural features were employed as input features. Morgan fingerprint,[37] a circular molecular fingerprint that takes into account the neighborhood of individual atoms, was chosen for this study. Each fingerprint contains a total of 1024 bits, each bit set to either 1 or 0. On the other hand, molecular graphs as such also serve as input features for one of the modeling methods employed in this study.

2.5. Modeling methods

2.5.1. Random forest

A random forest (RF)[38] is an ensemble of several decision trees that are fitted on random subsets of input features of the data set. The outcome is decided via a majority vote on the outcomes from the individual trees in the forest. Using this averaging approach, RF is robust to overfitting and thereby improves prediction accuracy. We used the '*RandomForestClassifier*' method implemented in Scikit-learn,[39] a Python library for machine learning. In this study we employed a total of 100 estimators (i.e., individual trees) per model. The '*random state*' parameter was set to an integer (random state = 42). The remaining parameters were set to default. We built RF models based on both RDKit descriptors and Morgan fingerprints.

Table 1
Overview of data sets employed for developing models in this study.

Dataset	Total Compounds	Class = 1 (Low Permeability)	Class = 0 (Moderate to High Permeability)
Training Set I	4181	566	3615
Training Set II	1698	566	1132
External Set	1046	141	905

2.5.2. XGBoost

eXtreme Gradient Boosting (XGBoost) is another method evaluated in this study. While RF builds a set of independent trees of unlimited depth, the gradient boosting technique builds a series of smaller trees where each tree corrects for the residuals in the previous tree's predictions. First implemented as Generalized Boosted Models (GBM), the method was considered to perform similarly to RF although the high number of adjustable parameters has limited its applicability on large datasets. Later, Chen and Guestrin implemented XGBoost[40] (https://github.com/dmlc/xgboost) which is based on the same idea behind GBM but uses an additive strategy to generate the prediction output. Furthermore, XGBoost uses a split-finding approach that can efficiently train on sparse data. This approach is particularly best suited when using sparse molecular representations such as fingerprints that contain many zeros. Due to its speed and widely recognized performance, we employed the XGBoost method using the same number of trees as RF. Both RDKit descriptors and Morgan fingerprints were employed.

2.5.3. Deep neural network

Artificial neural networks (ANNs) have been applied to a wide range of QSAR tasks. More recently, the ANNs have evolved into deep neural networks (DNN). Unlike an ANN, a DNN consists of multiple fully connected layers with two or more hidden layers between the input and output layers. In a feedforward neural network (referred to simply as DNN in the rest of the study), the information passed through the input layer flows in a forward direction through the hidden layers to the output layer. DNN models were implemented in Keras (https://keras.io) using the TensorFlow (https://tensorflow.org) backend. The number of hidden layers was adjusted based on the size of input descriptors (i.e., 119 for RDKit descriptors and 1024 for Morgan fingerprint).

2.5.4. Graph convolutional neural network

Graphs are natural ways to represent chemical structures where nodes represent atoms and edges represent the bonds between them. We recently showed that graph convolutional neural network (GCNN) provided superior performance in modeling Tier I ADME endpoints (rat liver microsomal stability, PAMPA permeability, and kinetic aqueous solubility).[41–42] A message passing variant of GCCN implemented in the ChemProp[43] Python package (https://github.com/chemprop/chemprop/) was employed to build GCNN models. The algorithm generates graph features when chemical structures (as line notations) and associated target values (i.e., PAMPA pH 5) are provided as input. The model parameters were set to default.

2.6. Modeling and validation

The training sets (I & II) were used to build models that were validated on the external set. Each training set was randomly divided into internal training and internal test sets (at an 80:20 ratio) for a total of five times. Each time, the model developed using the internal training set was validated on the internal test set. This procedure, widely known as *k*-fold ($k = 5$) cross-validation,[44] was employed to identify the best performing methods and descriptors. The best models identified from the cross-validation were further validated on the external set.

The model performance was assessed using different statistical measures. A receiver operating characteristic (ROC) curve, that plots true positive rate against the false positive rate, was used to estimate the predictive power of the classification models. The area under the ROC curve (i.e., AUC) is a numerical value between 0 and 1. The higher the value, the better the predictive power. Sensitivity indicates the proportion of true positives correctly predicted as positive. Specificity is the ability of the model to correctly predict true negatives as negative. Balanced accuracy (BACC) is an average of the Sensitivity and Specificity. It is a useful alternative to accuracy when the datasets in hand have a large degree of class imbalance. Cohen's *Kappa* is another metric used in this study that measures the agreement between the actual

classes and the classes predicted by the classifier. The equations for these measures are as follows:

$$Sensitivity = \frac{TP}{(TP + FN)}$$

$$Specificity = \frac{TN}{(FP + TN)}$$

$$Balanced\ accuracy = \frac{Sensitivity + Specificity}{2}$$

$$Kappa = \frac{p_a - p_\in}{1 - p_\in}$$

Here, TP = true positives, FN = false negatives, TN = true negatives, and FP = false positives. In the case of Kappa, p_a is the proportion of observations in agreement and $p_\in$ is the proportion in agreement due to chance.

3. Results

3.1. Assay performance

Three control compounds, ranitidine (low permeability), dexamethasone (moderate permeability), and verapamil (high permeability), were run with each plate to ensure assay quality. Table 2 shows the assay reproducibility data for these compounds, spanning 194 plates over 4 years. The minimum significant ratios (MSR)[45] for dexamethasone and verapamil were around 2.0, which indicate excellent assay reproducibility over time. Standard deviation (S.D.) and MSR value were not calculated for ranitidine as P_{eff} values are always below the limit of quantification.

3.2. Distribution of molecular properties

The greatest number of compounds in our dataset were found in the moderate/high permeability category (~72%) followed by the low permeability category (28%) (Fig. 1). Molecular properties, sLogP (Log P), total polar surface area (TPSA), and molecular weight (MW), were calculated using an *in-house* compound dataset annotation tool known as NCATS Find.[46] A large proportion of compounds from both P_{eff} categories fell within the 300–500 g/mol MW range, had Log P values between 2 and 6 and TPSA values less than 100. No significant differences were found between both categories based on the distribution of these molecular properties (Fig. 2).

3.3. Correlating PAMPA pH 5 permeability with oral bioavailability (%F)

Oral bioavailability (%F) is the fraction of an orally administered drug that reaches systemic circulation. To illustrate the application of our PAMPA pH 5 assay, we attempted to correlate log P_{eff} values with oral bioavailability (%F) obtained from *in-house* pharmacokinetic (PK) studies (128 compounds). This *in-house* PK database was built with studies in mice (90%) and rats (10%), from a variety of projects with intravenous (IV) doses ranging from 1 to 5 mg/kg and oral (PO) doses ranging from 3 to 50 mg/kg, the median dosages being 3 mg/kg. We set the %F cut-off values at 20% as it represents an acceptable criteria for screening compounds in drug discovery.[47,48]

Table 2
Reproducibility data for control compounds. Mean and S.D. permeability (P_{eff}) values were calculated across 194 plates.

Compound	P_{eff} (10^{-6} cm/s)	MSR ($10^{2\sqrt{[2]*S.D.}}$)
Ranitidine	<1	N/A
Dexamethasone	61 ± 16	2.3
Verapamil	208 ± 52	2.1

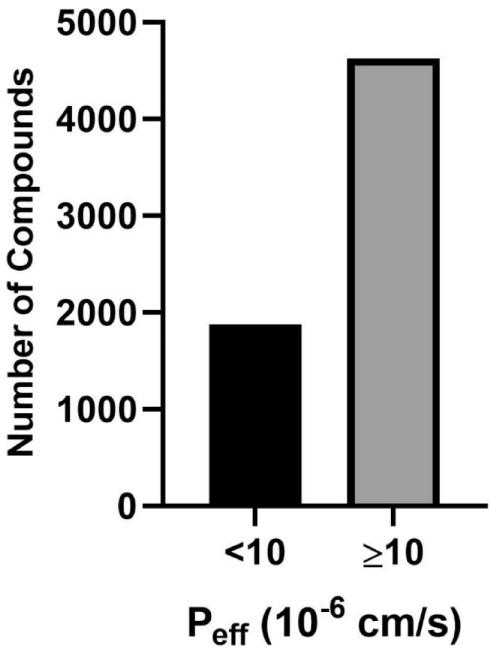

Fig. 1. Number of compounds categorized into low permeability (black), and moderate/high permeability (gray).

The cut-off value for the PAMPA assay was set at 10×10^{-6} cm/sec since it is the value differentiating compounds between low and moderate/high permeability. While we did not achieve a linear correlation, a categorical correlation of 74% was observed (Fig. 3A). %F is a complex property dependent on several factors such as GI physiology, physicochemical characteristics of the compound, drug metabolism, food, formulation, disease state, etc. Solubility and microsomal stability, two properties that affect %F, are also routinely tested for every compound synthesized at NCATS as part of Tier I ADME screening.[49,41] To understand if a better correlation with %F could be obtained, we filtered our 128-compound dataset and eliminated compounds with poor solubility (<10 μg/mL)[49] and poor microsomal stability ($t_{1/2}$ < 30 min)[41] (Fig. 3B). P_{eff} values for the remaining 62-compounds were correlated with %F and an improved correlation of ~85% was observed (Fig. 3C).

3.4. Cross-validation results

Training sets I and II were employed for 5-fold cross-validation (5-CV). DNN and GCNN models were compared with the baseline models based on RF and XGBoost. The baseline models RF and XGBoost provided similar performance on the training set I. Due to the high number of majority class examples in the dataset, the specificity values were high compared to sensitivity values. In the case of both RF and XGBoost, RDKit descriptors provided slightly better sensitivity values compared to Morgan fingerprints. In contrast, the DNN models provided better sensitivity values with Morgan fingerprints. The performance of GCNN was found to be similar to DNN.

When evaluated using training set II, the overall performance of all models improved on account of enhanced sensitivity due to a lower degree of class imbalance. The performance of RF and XGBoost models remained the same while DNN showed slightly better performance using RDKit descriptors compared to Morgan fingerprints. DNN and GCNN models provided a better balance between sensitivity and specificity. Figs. 4 and 5 provide a comparison of the performance of models based on different methods and descriptors in terms of balanced accuracy, sensitivity, and specificity. The complete 5-CV results are provided in the supplementary information.

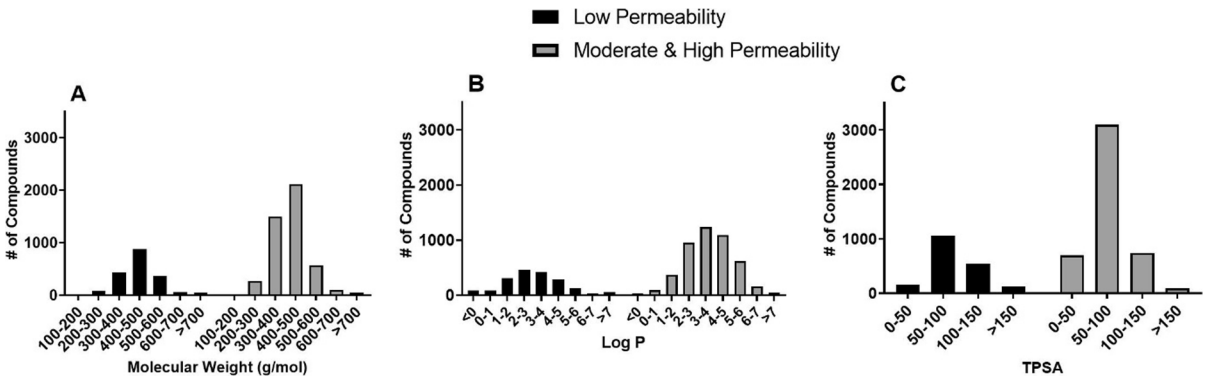

Fig. 2. Distribution of dataset based on A) Molecular Weight, B) Log P, and C) TPSA. Dataset is divided into compounds with low permeability (black) and compounds with moderate to high permeability (gray).

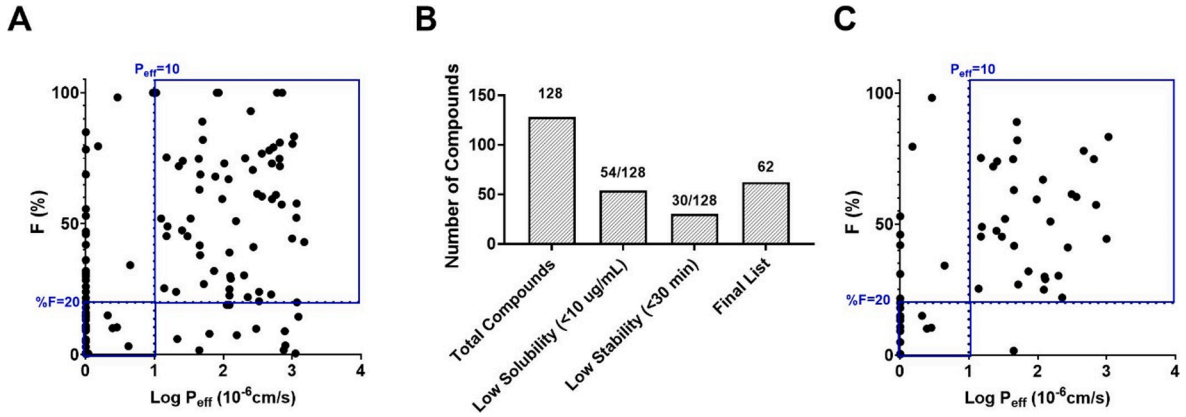

Fig. 3. Correlating log P_{eff} at pH 5 with %F. (A) %F vs Log P_{eff} with the 128-compound dataset. (B) Eliminating compounds with poor solubility and poor microsomal stability. (C) %F vs Log P_{eff} with the 62-compound dataset. Blue boxes in A and C show the categorical binning.

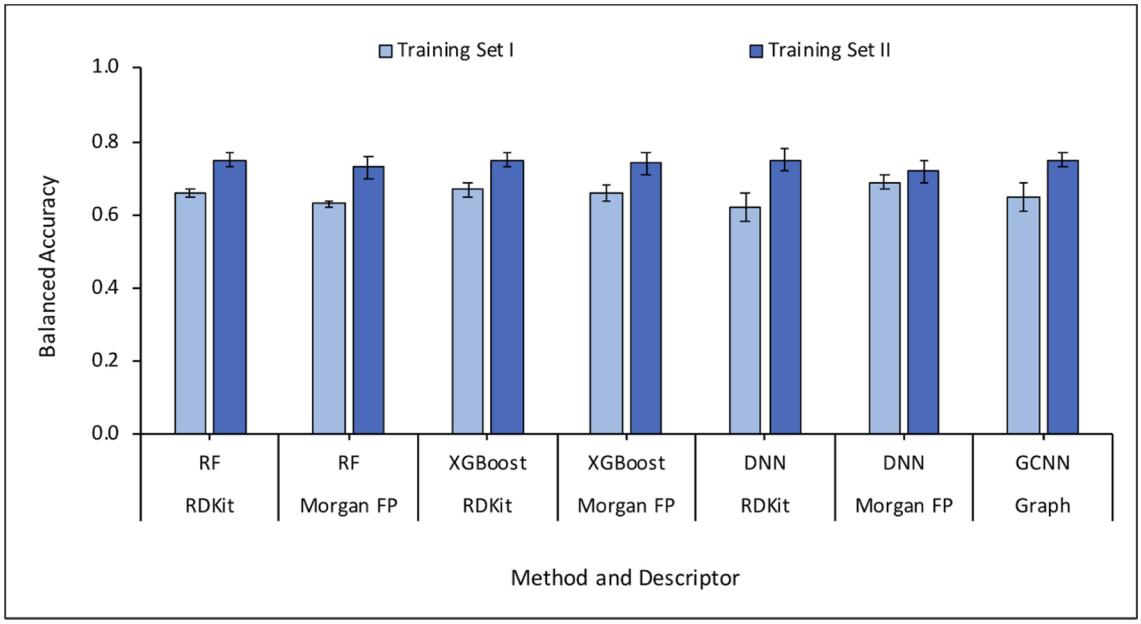

Fig. 4. Comparison of model performances in 5-fold cross-validation measured as balanced accuracies. Each error bar represents the standard deviation of the average of the performance in five folds.

3.5. External validation results

Since training set II provided better performance in cross-validation, we only used the models based on this dataset to predict the external set. Once again, RF and XGBoost provided higher specificity values compared to sensitivity and RDKit descriptors provided superior

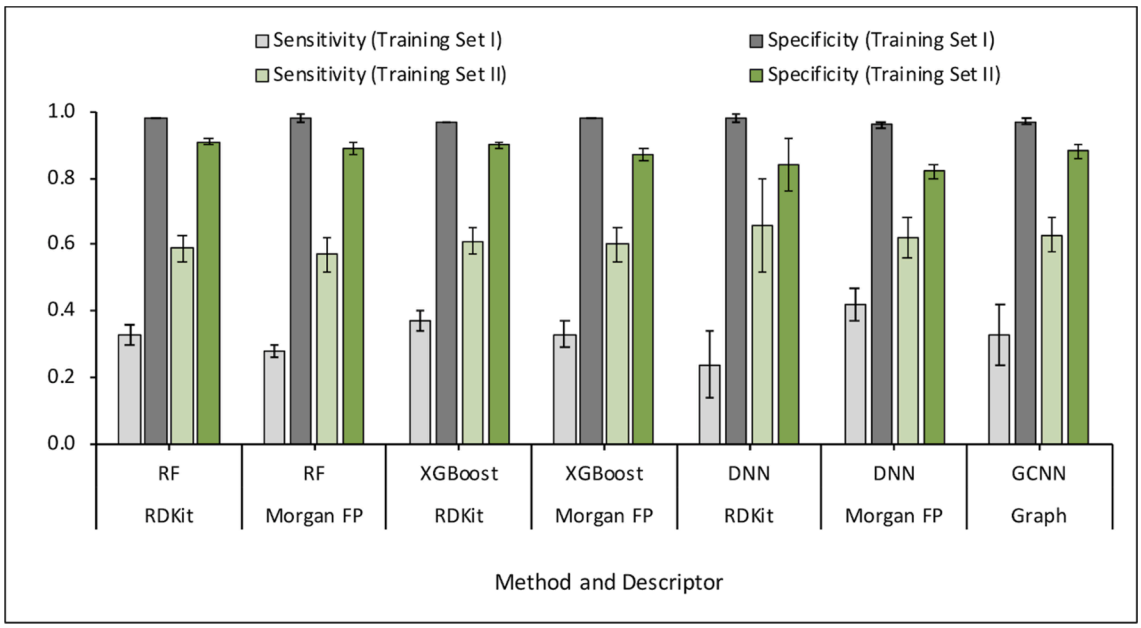

Fig. 5. Comparison of Sensitivity and Specificity values for training sets I and II. The error bars represent the standard deviations of average values for five folds.

performance over Morgan fingerprints. The DNN model based on Morgan fingerprints provided better balanced accuracy due to improved sensitivity. The GCNN model based on molecular graphs provided the best performance on the external set (Table 3).

3.6. Feature importance

We analyzed our data further to understand structural features and important properties that are indicative of poor PAMPA permeability. The GCNN architecture, as implemented in the ChemProp package, provides a mechanism for identifying substructural features that explain the molecular property. For each compound, the interpretation module provides a predicted property value along with a substructural feature and an associated rationale score. The rationale score is the predicted property value for the substructure. We identified 11 features that were present in at least 30 compounds (log frequency > 1.5) in the training set and were predicted to have a rationale score > 2.5 (Fig. 6). These substructures are overrepresented in compounds with moderate to high PAMPA permeability (log $P_{eff} > 2.5$) from the training data. We also identified substructures that were predicted to have a rationale score $<= 1$ and satisfy the frequency criterion (log frequency > 1.5). These substructures (Table 4) are overrepresented in compounds with low PAMPA permeability (log $P_{eff} < 1$) from our training data and can be of interest to medicinal chemists when dealing with liabilities due to PAMPA permeability. To the best of our knowledge, this is the first study to present analysis of substructural features relevant to PAMPA permeability. Closely examining the substructures reported in Fig 6 and Table 4 reveals that the latter comprise of a higher number of basic nitrogen atoms. Due to the presence of more polar groups, the latter substructures tend to be more water soluble which explains the poor lipophilicity, and hence permeability. Additionally, we found that the minimum and maximum SlogP values for the substructures on the higher end of the PAMPA permeability scale are 1.12 and 2.24 as compared to −0.55 and 0.97 for those on the lower end of the scale.

Similarly, we investigated the RF model to identify RDKit descriptors that were scored higher in terms of importance of the RDKit features. The complete dataset was used for this purpose and out of the 119 RDKit descriptors, a total of 48 descriptors were identified to have importance of at least 0.01. Out of the 48 descriptors, we closely examined 17 descriptors (Fig. 7) with an importance $>= 0.015$. As anticipated, Log P (calculated by RDKit as SlogP) turned out to be the most important feature (average feature importance of 0.03) for the classification model followed by peoe_VSA8, smr_VSA3, peoe_VSA2, and topological polar surface area (TPSA). Log P, Log D, and polar surface area have been previously discussed to be important descriptors for PAMPA permeability.[50–52] PEOE descriptors are those based on the partial charges of each atom in a molecule, calculated using Partial Equalization of Orbital Electronegativities (PEOE) method of calculating atomic partial charges, and depend only on the connectivity (i.e., elements, formal charges, and bond orders).

3.7. Validation using molecular weight and time split

We previously demonstrated using rat liver microsomal stability data that a time-based splitting of data provides an alternative assessment of model performance.[41] A recent study[53] proposed molecular weight split combined with time-based splitting as a cross-validation strategy to validate ADME prediction models. The authors removed compounds

Table 3
External validation performance of models built using training set II.

Method	Descriptor	AUC	BACC	Sensitivity	Specificity	Kappa
RF	RDKit	0.83	0.74	0.62	0.87	0.41
RF	Morgan FP	0.78	0.71	0.60	0.83	0.32
XGBoost	RDKit	0.83	0.77	0.69	0.86	0.44
XGBoost	Morgan FP	0.80	0.71	0.57	0.84	0.33
DNN	RDKit	0.80	0.70	0.50	0.90	0.37
DNN	Morgan FP	0.77	0.73	0.64	0.82	0.34
GCNN	Graph	0.84	0.78	0.74	0.82	0.40

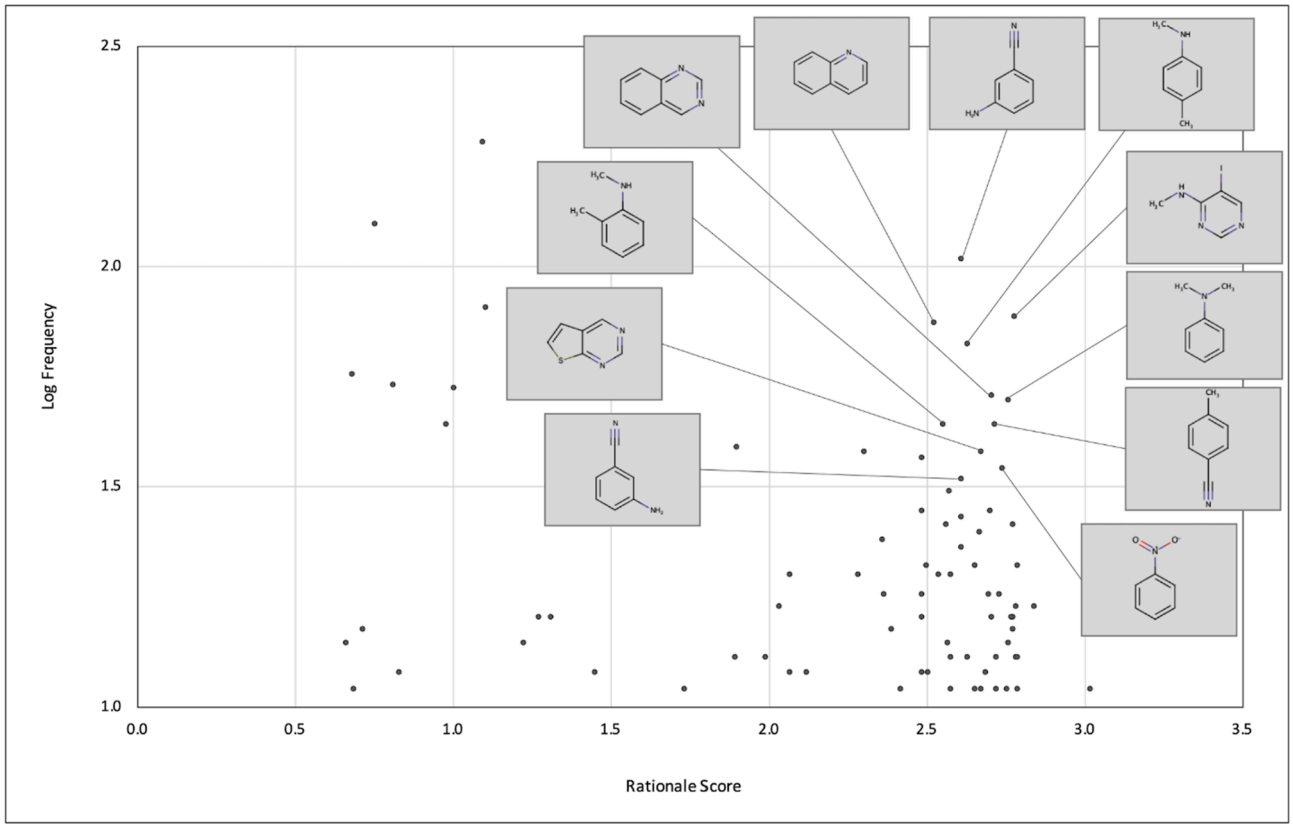

Fig. 6. Features interpreted by the GCNN model. X-axis stands for the rationale score and Y-axis stands for the frequency of the feature in logarithmic scale. The top 11 features are shown on the plot.

Table 4
Substructural features from GCNN model that represent low permeability compounds.

Substructure	Rationale Score	Frequency
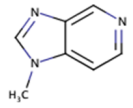	0.68	57
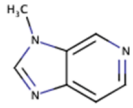	0.75	125
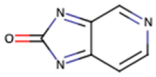	0.82	54
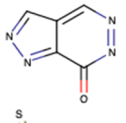	1.01	51
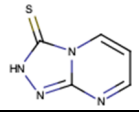	0.98	44

with molecular weight higher than 500 g/mol from the training set and retained only those compounds with molecular weight higher than 600 g/mol in the external set. In the current study, we have data spanning 2016, 2017, 2018, and 2019 with approximately 25% of the data coming from the year 2019. Therefore, using the data from the years 2016, 2017, and 2018 as the training set and the rest as the external set closely resembles a random split of the data set at 80:20 ratio that resulted in the original external set. Additionally, we removed compounds with molecular weight > 500 g/mol from the training set and slightly adjusted the original criterion to retain compounds with weight > 550 g/mol in the external set. The reason behind adjusting this criterion is to accommodate a higher number of compounds in the external set. After temporal and molecular weight split, the training and external sets comprised of 3334 (Class 1: 407; Class 0: 2927) compounds and 119 (Class 1: 19; Class 0: 100) compounds, respectively. This model provided a balanced accuracy of 65% (Sensitivity: 58% and Specificity: 73%). While the performance is inferior compared to the performance of models on the other external set, this could be explained by the presence of unusually large molecules (average molecular weight = 885 Daltons and average number of rings per molecule = 6) in comparison to the corresponding training set (average molecular weight = 400 Daltons and average number of rings per molecule = 4). It would be worth investigating this strategy on a larger dataset that spans multiple years and a wider chemical space.

4. Discussion

Oral bioavailability is a complex process dependent on many physiological, physicochemical, and pharmacological parameters including membrane permeability, solubility, metabolic stability, particle size, pH, surface area of the GI tract, activities of uptake and efflux transporters, etc. For an orally administered drug to reach systemic circulation, it must pass through the intestinal membrane by passive diffusion, carrier mediated uptake, or active transport mechanisms. Cell-based assays, such as Caco-2 and MDCK cell culture systems, have been used to model membrane permeability and these assays have become the standard in the pharmaceutical industry. However, since 80–95% of commercially available drugs are absorbed via passive diffusion,[2,17,19,20,18] PAMPA is a popular alternative approach. PAMPA has several advantages including low cost, amenability to high-throughput, shorter lead times,

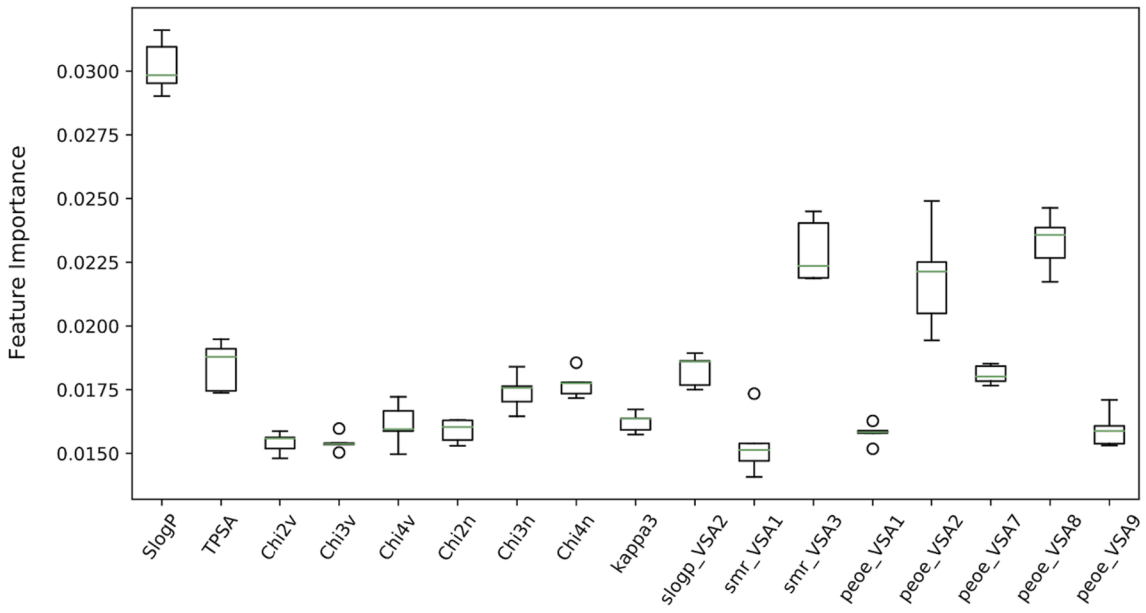

Fig. 7. RDKit descriptors identified as important features by RF model based on 5-CV using the complete dataset. For each descriptor, the feature importance score from the five folds is plotted.

as well as comparable prediction accuracy to the Caco-2 assay for prediction of intestinal permeability.[54] Additionally, the good day-to-day reproducibility and lower data variability[54] make datasets generated through PAMPA assays highly sought after for *in silico* QSAR modeling. In this study, we used our 6500 compound PAMPA pH 5 dataset and built classification models to predict intestinal permeability of test compounds. While a few PAMPA QSAR models exist in literature, they are built using relatively small datasets and neither the model nor the datasets have been made publicly available. While we cannot make our entire dataset public due to its proprietary nature, a small subset (486 compounds; PubChem AID: 1645871) of our data and the best predictive models have been made public. Our PAMPA models (pH 5 and pH 7.4; published previously[18] are to the best of our knowledge, the only open-access PAMPA models built using high-quality data and generated at a single laboratory.

A recent study by Oja and Maran highlighted the importance of understanding the pH-permeability relationship, especially for ionizable compounds.[2] They also emphasized the fact that most PAMPA studies in literature have been performed at neutral or near-neutral pH and thus, there is a dearth of PAMPA permeability data and QSAR models at different pH values. To this end, Oja and Maran have published datasets and QSAR models (238 compounds) for PAMPA permeability at pH 3, 5, 7.4 and 9.[22] Our PAMPA datasets go a long way towards filling this data gap. Although the openly accessible compounds represent a relatively small percentage of our total dataset, these represent by far, the largest datasets in literature (Table 5).

Multiple studies reported QSAR models to predict PAMPA permeability.[55–57,23,58–61,19,18,22] However, as emphasized earlier by Chi et al,[62] PAMPA permeability depends on several factors other than the pH of the assay. Therefore, creating a good QSAR model using data available in the public domain has been considered impractical. Most previously reported models were based on linear regression techniques such as partial least squares (PLS) and multiple linear regression. Later, having understood that there exists a bilinear relationship between Log D and PAMPA permeability, it became clear that the linear regression models were unable to capture the complex nonlinearity.[63] Machine learning methods such as support vector machines, random forests and gradient boosting have been employed[64,62,65] using both public and proprietary datasets. Though most studies reported regression models, a few studies reported categorical models using classification criteria similar to those employed in the current study.[55,66,67] While most studies relied on a handful of physicochemical properties, some of them employed large numbers of 2D or 3D descriptors from commercial software. Considering that type of assay used in our study (double sink PAMPA) is different from other published studies and that there are very few PAMPA studies conducted at pH 5, we could not directly compare our models with those in literature.

Additionally, we correlated the PAMPA pH 5 permeability values with preclinical oral bioavailability and observed an accuracy of 74%. Considering that oral bioavailability is an extremely complex and multifactorial property, this correlation was encouraging. Moreover, after accounting for solubility and metabolic stability, two parameters that affect oral bioavailability, this correlation increased to 85%. The corresponding correlation for the PAMPA pH 7.4 dataset was found to be 80% (unpublished data). This suggests that the proper use of our data and models could help minimize the risk of compounds failing in preclinical *in vivo* studies due to poor bioavailability.

Table 5
Summary of NCATS ADME Models and Datasets.

Assay	Type	Number of Compounds	Location
PAMPA pH 5	Dataset	486	PubChem- AID: 1645871
PAMPA pH 5	Model	6500	https://opendata.ncats.nih.gov/adme/
PAMPA pH 7.4	Dataset	2532	PubChem- AID: 1508612
PAMPA pH 7.4[42]	Model	22,000	https://opendata.ncats.nih.gov/adme/

5. Conclusion

In summary, we developed a robust QSAR model using our PAMPA pH 5 dataset and identified structural features and descriptors relevant for PAMPA pH 5 permeability. An extensive analysis comparing the more recent graph convolutional neural network with the state-of-the-art methods such as random forests revealed that the graph-based method provides superior predictive performance in identifying compounds with low PAMPA permeability and distinguishing them from those with moderate or high PAMPA permeability. We also discussed the

substructures that prominently appeared in both poor and high permeability compounds as predicted by the graph neural network model. This model along with our previously published ADME QSAR models[42] (https://opendata.ncats.nih.gov/adme) can be used to rank-order compounds for synthesis and thus, project teams can get to their optimized lead compounds in fewer iterations. Furthermore, the ~85% correlation observed between PAMPA permeability at pH 5 and *in vivo* oral bioavailability grants medicinal chemists the confidence to move compounds forward onto preclinical testing quickly. Overall, implementing *in silico* tools in early drug discovery may ultimately prove to be game changing in the time-intensive, costly, and high-attrition drug discovery and development process.

Availability of data and materials

The dataset supporting the conclusions of this article is available in the PubChem repository, Assay ID 1645871. The models supporting the conclusions of this article are available in the Open Data NCATS ADME portal (ADME@NCATS), https://opendata.ncats.nih.gov/adme/. An Excel sheet containing the complete 5-fold cross-validation results for Training Set I & II and a pair-wise comparison of all the machine learning methods utilized is submitted as supplementary information.

Funding

This research was supported in part by the Intramural Research Program of the National Institutes of Health, National Center for Advancing Translational Sciences.

Declaration of Competing Interest

The authors declare that they have no known competing financial interests or personal relationships that could have appeared to influence the work reported in this paper.

Acknowledgements

The authors would like to acknowledge Cordelle Tanega at NCATS for helping with the deposition of data in the PubChem bioassay database.

Appendix A. Supplementary material

Supplementary data to this article can be found online at https://doi.org/10.1016/j.bmc.2021.116588.

References

[1] Oja M, Sild S, Maran U. Logistic Classification Models for pH-Permeability Profile: Predicting Permeability Classes for the Biopharmaceutical Classification System. *J Chem Inf Model*. 2019;59:2442–2455. https://doi.org/10.1021/acs.jcim.8b00833.

[2] Oja M, Maran U. The Permeability of an Artificial Membrane for Wide Range of pH in Human Gastrointestinal Tract: Experimental Measurements and Quantitative StructureActivity Relationship. *Mol Inf*. 2015;34:493–506. https://doi.org/10.1002/minf.201400147.

[3] Volpe DA. Drug-permeability and transporter assays in Caco-2 and MDCK cell lines. *Future Med Chem*. 2011;3:2063–2077. https://doi.org/10.4155/fmc.11.149.

[4] Lennernas H. Regional intestinal drug permeation: biopharmaceutics and drug development. *Eur J Pharm Sci*. 2014;57:333–341. https://doi.org/10.1016/j.ejps.2013.08.025.

[5] Dahlgren D, Roos C, Lundqvist A, et al. Regional Intestinal Permeability of Three Model Drugs in Human. *Mol Pharm*. 2016;13:3013–3021. https://doi.org/10.1021/acs.molpharmaceut.6b00514.

[6] Charman WN, Porter CJ, Mithani S, Dressman JB. Physiochemical and physiological mechanisms for the effects of food on drug absorption: the role of lipids and pH. *J Pharm Sci*. 1997;86:269–282. https://doi.org/10.1021/js960085v.

[7] Avdeef A. *Absorption and Drug Development. Solubility, Permeability, and Charge State*. 2nd ed. Hoboken, New Jersey: John Wiley & Sons; 2012.

[8] Vertzoni M, Augustijns P, Grimm M, et al. Impact of regional differences along the gastrointestinal tract of healthy adults on oral drug absorption: An UNGAP review. *Eur J Pharm Sci*. 2019;134:153–175. https://doi.org/10.1016/j.ejps.2019.04.013.

[9] Shore PA, Brodie BB, Hogben CA. The gastric secretion of drugs: a pH partition hypothesis. *J Pharmacol Exp Ther*. 1957;119:361–369.

[10] Grasset E, Pinto M, Dussaulx E, Zweibaum A, Desjeux JF. Epithelial properties of human colonic carcinoma cell line Caco-2: electrical parameters. *Am J Physiol*. 1984;247:C260–C267. https://doi.org/10.1152/ajpcell.1984.247.3.C260.

[11] Artursson P, Karlsson J. Correlation between oral drug absorption in humans and apparent drug permeability coefficients in human intestinal epithelial (Caco-2) cells. *Biochem Biophys Res Commun*. 1991;175:880–885. https://doi.org/10.1016/0006-291X(91)91647-U.

[12] Lennernäs H, Palm K, Fagerholm U, Artursson P. Comparison between active and passive drug transport in human intestinal epithelial (caco-2) cells in vitro and human jejunum in vivo. *Int J Pharm*. 1996;127:103–107. https://doi.org/10.1016/0378-5173(95)04204-0.

[13] Putnam WS, Pan L, Tsutsui K, Takahashi L, Benet LZ. Comparison of Bidirectional Cephalexin Transport Across MDCK and Caco-2 Cell Monolayers: Interactions with Peptide Transporters. *Pharm Res*. 2002;19:27–33. https://doi.org/10.1023/A:1013647114152.

[14] D'Souza VM, Shertzer HG, Menon AG, Pauletti GM. High Glucose Concentration in Isotonic Media Alters Caco-2 Cell Permeability. *AAPS PharmSci*. 2003;5. https://doi.org/10.1208/ps050324.

[15] Bravo SA, Nielsen CU, Amstrup J, Frokjaer S, Brodin B. In-depth evaluation of Gly-Sar transport parameters as a function of culture time in the Caco-2 cell model. *Eur J Phram Sci*. 2004;21:77–86. https://doi.org/10.1016/s0928-0987(03)00205-7.

[16] Anderle P, Niederer E, Rubas W, et al. P-Glycoprotein (P-gp) mediated efflux in Caco-2 cell monolayers: the influence of culturing conditions and drug exposure on P-gp expression levels. *J Pharm Sci*. 1998;87:757–762. https://doi.org/10.1021/js970372e.

[17] Avdeef A. The rise of PAMPA. *Expert Opin Drug Metab Toxicol*. 2005;1:325–342. https://doi.org/10.1517/17425255.1.2.325.

[18] Sun H, Nguyen K, Kerns E, et al. Highly predictive and interpretable models for PAMPA permeability. *Bioorg Med Chem*. 2017;25:1266–1276. https://doi.org/10.1016/j.bmc.2016.12.049.

[19] Oja M, Maran U. Quantitative structure-permeability relationships at various pH values for acidic and basic drugs and drug-like compounds. *SAR QSAR Environ Res*. 2015;26:701–719. https://doi.org/10.1080/1062936X.2015.1085896.

[20] Kerns E, Di L, Petusky S, Farris M, Ley R, Jupp P. Combined Application of Parallel Artificial Membrane Permeability Assay and Caco-2 Permeability Assay in Drug Discovery. *J Pharm Sci*. 2004;93:1440–1453. https://doi.org/10.1002/jps.20075.

[21] Brennan MB. Drug Discovery - filtering out failures early in the game. Chem Eng News, vol. 78. American Chemical Society; 2000.

[22] Oja M, Maran U. pH-permeability profiles for drug substances: Experimental detection, comparison with human intestinal absorption and modelling. *Eur J Pharm Sci*. 2018;123:429–440. https://doi.org/10.1016/j.ejps.2018.07.014.

[23] Verma RP, Hansch C, Selassie CD. Comparative QSAR studies on PAMPA/modified PAMPA for high throughput profiling of drug absorption potential with respect to Caco-2 cells and human intestinal absorption. *J Comput Aided Mol Des*. 2007;21:3–22. https://doi.org/10.1007/s10822-006-9101-z.

[24] Frings M, Bolm C, Blum A, Gnamm C. Sulfoximines from a Medicinal Chemist's Perspective: Physicochemical and in vitro Parameters Relevant for Drug Discovery. *Eur J Med Chem*. 2017;126:225–245. https://doi.org/10.1016/j.ejmech.2016.09.091.

[25] Yamaki S, Suzuki D, Fujiyasu J, et al. Synthesis and structure activity relationships of glycine amide derivatives as novel Vascular Adhesion Protein-1 inhibitors. *Bioorg Med Chem*. 2017;25:187–201. https://doi.org/10.1016/j.bmc.2016.10.025.

[26] Furukawa A, Townsend CE, Schwochert J, Pye CR, Bednarek MA, Lokey RS. Passive Membrane Permeability in Cyclic Peptomer Scaffolds Is Robust to Extensive Variation in Side Chain Functionality and Backbone Geometry. *J Med Chem*. 2016;59:9503–9512. https://doi.org/10.1021/acs.jmedchem.6b01246.

[27] Zhang X, Glunz PW, Johnson JA, et al. Discovery of a Highly Potent, Selective, and Orally Bioavailable Macrocyclic Inhibitor of Blood Coagulation Factor VIIa-Tissue Factor Complex. *J Med Chem*. 2016;59:7125–7137. https://doi.org/10.1021/acs.jmedchem.6b00469.

[28] Grosche P, Sirockin F, Mac Sweeney A, et al. Structure-based design and optimization of potent inhibitors of the adenoviral protease. *Bioorg Med Chem Lett*. 2015;25:438–443. https://doi.org/10.1016/j.bmcl.2014.12.057.

[29] Flanders Y, Dumas S, Caserta J, et al. A versatile synthesis of novel pan-PIM kinase inhibitors with initial SAR study. *Tetrahedron Lett*. 2015;56:3186–3190. https://doi.org/10.1016/j.tetlet.2015.01.119.

[30] Kim J, Chin J, Im CY, et al. Synthesis and biological evaluation of novel 4-hydroxytamoxifen analogs as estrogen-related receptor gamma inverse agonists. *Eur J Med Chem*. 2016;120:338–352. https://doi.org/10.1016/j.ejmech.2016.04.076.

[31] Chan HCS, Shan H, Dahoun T, Vogel H, Yuan S. Advancing Drug Discovery via Artificial Intelligence. *Trends Pharmacol Sci*. 2019;40:592–604. https://doi.org/10.1016/j.tips.2019.06.004.

[32] Avdeef A, Artursson P, Neuhoff S, Lazorova L, Grasjo J, Tavelin S. Caco-2 permeability of weakly basic drugs predicted with the double-sink PAMPA pKa (flux) method. *Eur J Pharm Sci*. 2005;24:333–349. https://doi.org/10.1016/j.ejps.2004.11.011.

[33] Bennion BJ, Be NA, McNerney MW, et al. Predicting a Drug's Membrane Permeability: A Computational Model Validated With in Vitro Permeability Assay Data. *J Phys Chem B*. 2017;121:5228–5237. https://doi.org/10.1021/acs.jpcb.7b02914.

[34] Shah P, Kerns E, Nguyen DT, et al. An Automated High-Throughput Metabolic Stability Assay Using an Integrated High-Resolution Accurate Mass Method and Automated Data Analysis Software. *Drug Metab Dispos*. 2016;44:1653–1661. https://doi.org/10.1124/dmd.116.072017.
[35] Fourches D, Muratov E, Tropsha A. Trust, but Verify II: A Practical Guide to Chemogenomics Data Curation. *J Chem Inf Model*. 2016;56:1243–1252. https://doi.org/10.1021/acs.jcim.6b00129.
[36] Shah P, Siramshetty VB, Zakharov AV, Southall NT, Xu X, Nguyen DT. Predicting liver cytosol stability of small molecules. *J Cheminf*. 2020;12:21. https://doi.org/10.1186/s13321-020-00426-7.
[37] Morgan HL. The Generation of a Unique Machine Description for Chemical Structures - A Technique Developed at Chemical Abstracts Service. *J Chem Doc*. 1965;5:107–113. https://doi.org/10.1021/c160017a018.
[38] Breiman L. Random Forests. *Machine Learning*. 2001;45:5–32. https://doi.org/10.1023/A:1010933404324.
[39] Pedregosa F, Varoquaux G, Gramfort A, et al. Scikit-learn: Machine Learning in {P}ython. *J Mach Learn Res*. 2011;12:2825–2830.
[40] Chen T, Guestrin C. XGBoost: A Scalable Tree Boosting System. Paper presented at the Proceedings of the 22nd ACM SIGKDD International Conference on Knowledge Discovery and Data Mining, San Francisco, California, USA; 2016.
[41] Siramshetty VB, Shah P, Kerns E, et al. Retrospective assessment of rat liver microsomal stability at NCATS: data and QSAR models. *Sci Rep*. 2020;10:20713. https://doi.org/10.1038/s41598-020-77327-0.
[42] Siramshetty VB, Williams J, Nguyen D, Neyra J, Southall N, Mathe E, Xu X, Shah P. Validating ADME QSAR Models Using Marketed Drugs. *SLAS Discovery: Adv Sci Drug Discovery*. 2021. https://doi.org/10.1177/24725552211017520.
[43] Chemprop/chemprop Message Passing Neural Networks for Molecule Property Prediction.
[44] Refaeilzadeh P, Tang L, Liu H. Cross-Validation. In: Liu L, ÖZsu MT (Eds.), Encyclopedia of Database Systems. Springer US, Boston, MA; 2009. p. 532–8. doi: 10.1007/978-0-387-39940-9_565.
[45] Assay Guidance Manual. Eli Lilly & Company and the National Center for Advancing Translational Sciences, Bethesda, MD; 2004.
[46] NCATS Resolver. https://tripod.nih.gov/servlet/resolver/.
[47] Hou T, Wang J, Zhang W, Xu X. ADME Evaluation in Drug Discovery. 6. Can Oral Bioavailability in Humans Be Effectively Predicted by Simple Molecular Property-Based Rules? *J Chem Inf Model*. 2007;47:460–463. https://doi.org/10.1021/ci6003515.
[48] Veber DF, Johnson SR, Chen H-Y, Smith BR, Ward KW, Kopple KD. Molecular Properties That Influence the Oral Bioavailability of Drug Candidates. *J Med Chem*. 2002;45:2615–2623. https://doi.org/10.1021/jm020017n.
[49] Sun H, Shah P, Nguyen K, et al. Predictive models of aqueous solubility of organic compounds built on a large dataset of high integrity. *Bioorg Med Chem*. 2019;27:3110–3114. https://doi.org/10.1016/j.bmc.2019.05.037.
[50] Zhu C, Jiang L, Chen T, Hwang K. A comparative study of artificial membrane permeability assay for high throughput profiling of drug absorption potential. *Eur J Med Chem*. 2002;37:399–407. https://doi.org/10.1016/s0223-5234(02)01360-0.
[51] Flaten GE, Dhanikula AB, Luthman K, Brandl M. Drug permeability across a phospholipid vesicle based barrier: a novel approach for studying passive diffusion. *Eur J Pharm Sci*. 2006;27:80–90. https://doi.org/10.1016/j.ejps.2005.08.007.
[52] Over B, Matsson P, Tyrchan C, et al. Structural and conformational determinants of macrocycle cell permeability. *Nat Chem Biol*. 2016;12:1065–1074. https://doi.org/10.1038/nchembio.2203.
[53] Feinberg EN, Joshi E, Pande VS, Cheng AC. Improvement in ADMET Prediction with Multitask Deep Featurization. *J Med Chem*. 2020;63:8835–8848. https://doi.org/10.1021/acs.jmedchem.9b02187.
[54] Sugano K, Okazaki A, Sugimoto S, Tavornvipas S, Omura A, Mano T. Solubility and Dissolution Profile Assessment in Drug Discovery. *Drug Metab Pharmacokinet*. 2007;22:225–254. https://doi.org/10.2133/dmpk.22.225.
[55] Chaturvedi PR, Decker CJ, Odinecs A. Prediction of pharmacokinetic properties using experimental approaches during early drug discovery. *Curr Opin Chem Biol*. 2001;5:452–463. https://doi.org/10.1016/s1367-5931(00)00228-3.
[56] Ano R, Kimura Y, Shima M, Matsuno R, Ueno T, Akamatsu M. Relationships between structure and high-throughput screening permeability of peptide derivatives and related compounds with artificial membranes: application to prediction of Caco-2 cell permeability. *Bioorg Med Chem*. 2004;12:257–264. https://doi.org/10.1016/j.bmc.2003.10.002.
[57] Dibbell DG, Cohn R. Perforation of the colon during hydrostatic reduction. *Am J Surg*. 1966;115:715–717. https://doi.org/10.1016/0002-9610(66)90048-1.
[58] Fujikawa M, Nakao K, Shimizu R, Akamatsu M. QSAR study on permeability of hydrophobic compounds with artificial membranes. *Bioorg Med Chem*. 2007;15:3756–3767. https://doi.org/10.1016/j.bmc.2007.03.040.
[59] Kalyanaraman C, Jacobson MP. An atomistic model of passive membrane permeability: application to a series of FDA approved drugs. *J Comput Aided Mol Des*. 2007;21:675–679. https://doi.org/10.1007/s10822-007-9141-z.
[60] Nakao K, Fujikawa M, Shimizu R, Akamatsu M. QSAR application for the prediction of compound permeability with in silico descriptors in practical use. *J Comput Aided Mol Des*. 2009;23:309–319. https://doi.org/10.1007/s10822-009-9261-8.
[61] Akamatsu M, Fujikawa M, Nakao K, Shimizu R. In silico prediction of human oral absorption based on QSAR analyses of PAMPA permeability. *Chem Biodivers*. 2009;6:1845–1866. https://doi.org/10.1002/cbdv.200900112.
[62] Chi CT, Lee MH, Weng CF, Leong MK. In Silico Prediction of PAMPA Effective Permeability Using a Two-QSAR Approach. *Int J Mol Sci*. 2019;20. https://doi.org/10.3390/ijms20133170.
[63] Kansy M, Fischer H, Kratzat K, Senner F, Wagner B, Parrilla I. Pharmacokinetic Optimization in Drug Research. In: Testa B, van de Waterbeemd H, Folkers G, Guy R (Eds.), Pharmacokinetic Optimization in Drug Research; 2001. p. 447–64. doi: 10.1002/9783906390437.ch24.
[64] Sherer EC, Verras A, Madeira M, et al. QSAR Prediction of Passive Permeability in the LLC-PK1 Cell Line: Trends in Molecular Properties and Cross-Prediction of Caco-2 Permeabilities. *Mol Inf*. 2012;31:231–245. https://doi.org/10.1002/minf.201100157.
[65] Gousiadou C, Doganis P, Sarimveis H. Development of QSAR ensemble models for predicting the PAMPA Effective Permeability of new, non-peptidic leads with potential antiviral activity against the coronavirus SARS-CoV-2; 2021. doi: 10.3762/bxiv.2021.22.v1.
[66] Mahar Doan KM, Humphreys JE, Webster LO, et al. Passive permeability and P-glycoprotein-mediated efflux differentiate central nervous system (CNS) and non-CNS marketed drugs. *J Pharmacol Exp Ther*. 2002;303:1029–1037. https://doi.org/10.1124/jpet.102.039255.
[67] Wager TT, Hou X, Verhoest PR, Villalobos A. Moving beyond rules: the development of a central nervous system multiparameter optimization (CNS MPO) approach to enable alignment of druglike properties. *ACS Chem Neurosci*. 2010;1:435–449. https://doi.org/10.1021/cn100008c.